# Structural and AC conductivity of polyaniline doped nickle oxide nanocomposites

A. Zia[a], M. Irfan[c,*], S. Saeed[b], W. Abbas[c,†], M. Ehsan Mazhar[c], A. Waheed[d], M. Nisa[e], A. Riaz[e], S. Malik[e], N. Bano[f], I. Hussain[g], and S. Haider[c]

[a]*School of Optical Engineering, Beijing University of Technology, Beijing 100000, China.*
[b]*International Research Centre for Nano Handling and Manufacturing of China, Changchun University of Science and Technology, Changchun 130022, China.*
[c]*Institute of Physics, Bahauddin Zakriya University, Multan 60800, Pakistan.*
*e-mail: *mirfanphysics@gmail.com; †Dr.waseemabbas@bzu.edu.pk*
[d]*Civil Engineering Department NFC-IET, Multan 60800, Pakistan.*
[e]*Department of physics, Govt Sadiq College Women University BWP, 63100, Pakistan.*
[f]*Department of Physics & Astronomy, College of Science, King Saud University, P.O. Box2455, Riyadh 11451, Saudi Arabia.*
[g]*ETHICSS International Centre for Sustainability and Security 21 Colliston Drive Broughty Ferry Dundee DD5 3TL UK.*

Received 1 April 2024; accepted 9 November 2024

In this work, we have investigated the influence of polyaniline on the structural and electrical properties of polyaniline-nickel oxide (PANI-NiO) nanocomposites prepared by in-situ chemical polymerization. The experimental procedure involved the synthesis of Polyaniline (PANI) and their nanocomposites with varying weight percentages of NiO nanoparticles using an in-situ polymerization route. The structure of NiO@PANI nanocomposites was verified using the X-ray diffraction technique.

It was observed that NiO exhibited a single-crystalline structure, whereas PANI displayed a non-crystalline structure. Scanning electron microscopy (SEM) revealed spherical NiO and granular PANI, both with homogeneous distribution, and increased polymer content resulted in more porosity. The measured values of dielectric constant, dielectric loss, and AC conductivity decreased as frequency and temperature increased. The optimum presence of conductive PANI with nickel oxide in a nanocomposite is responsible for the increase in AC electrical conductivity. The prepared nanocomposite material behaves as a semiconductor and may be helpful for charge storage devices and related field applications.

*Keywords:* Polyaniline; polymer composite; in-situ polymerization; structural; electrical properties.

DOI: https://doi.org/10.31349/RevMexFis.71.020502

## 1. Introduction

Metal oxide (MOx) polymer composites attracted extensive consideration because of their remarkable electrical characteristics. These composite materials are composed of metal oxide nanoparticles that are incorporated into a polymer matrix. The properties of these composites can be customized to suit specific applications. Polyaniline (PANI) stands out as a preferred polymer due to its ease of synthesis, low density, cost-effectiveness, solubility in solvents, excellent processability, and excellent conducting attributes [1-3]. PANI exhibits remarkable conductivity, especially in its impure form, finding diverse applications such as electrodes, electromagnetic shielding, and antistatic coatings. While PANI serves specific electrochemical purposes, it is considered inferior to silver, which excels in accuracy compared to copper and is widely used in electronic circuit production and corrosion prevention [4]. Polyaniline is widely used in Organic LED [5], Electromagnetic shielding, bio-sensors [6-7], solar cells/batteries [8], artificial muscle [9], and Gate Oxide [10-11]. The electrical conductivity of metal oxide/polyaniline (PANI) composites can be adjusted by altering the concentration of metal oxide nanoparticles (MOx NPs) within the polymer matrix. This property renders these composites well-suited for gas-sensing applications [12-13].These composites exhibit a dual functionality, combining photoconductivity and electrical activity, making them useful as redox biomaterials for sensors. Due to its versatile applications, researchers have focused significantly on creating nanocomposites using PANI [14-15]. The presence of attractive Nano-structure filler particles enhances both the attraction and transport properties of the polymer in this form of nanocomposite [16].

In addition, NiO demonstrates antiferromagnetic characteristics and is a transition metal oxide with a band gap of 3.51 eV [17]. The nanoparticles have exceptional thermal stability. Additionally, this can enhance the thermal stability of PANI. Researchers have reported on the creation, characterization, fabrication, and influence of NiO NPs embedded PANI nanocomposites for desired electrical properties [18]. During the investigation, it was observed that the size of the particles had a significant impact on the appealing properties of NiO nanoparticles. Particles of tiny dimensions have a significant interface area between the ferromagnetic and antiferromagnetic states. The disruption of the structure and the interaction between different components eventually intensify as the interface or boundary region expands [19]. In literature [20], multiple effective techniques are documented for creating metal oxide/polymer nanocomposites. These methods include the sol-gel [21], compression molding [22], melt blending, co-precipitation [23], electrospinning, and

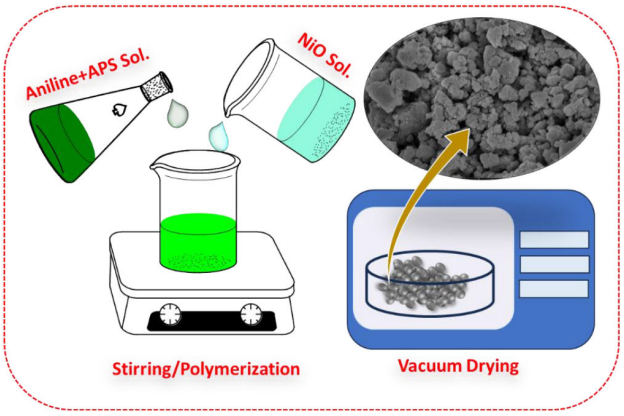


FIGURE 1. Synthesis Scheme of NiO@PANI nanocomposites.

layer-by-layer assembly [24]. Nevertheless, to improve the electrical conductivity and mechanical strength of MOx NPs/polymer hybrids, it is crucial to achieve a uniform dispersion of MOx NPs throughout the polymer matrix while also preserving the structural integrity of the polymer matrix and controlling the size and morphology of the MOx NPs [25]. These are the primary challenges that need to be addressed to achieve enhanced electrical conductivity and mechanical strength [26]. Thus, it is imperative to produce MOx NPs/polymer hybrids through precise polymerization and structural alterations to ensure their appropriate use [27-28]. In this work, we present the synthesis of NiO@PANI nanocomposites via in-situ polymerization method. We analyzed and compared the structural and electrical characteristics of NiO@PANI nanocomposite samples with various weight percentages of PANI.

## 2. Experimental details

Aniline was bought from Riedel-de-Haen ($>$ 99 % purity) Ammonium persulfate deliver by Duksan chemicals ($>$ 99 % purity). The Nickle Oxide was bought from UNI-CHcM chemicals (99.9 % purity) and Hydrochloric acid purchase from Sacharlu (99.9 % purity). All material was employed conventionally except aniline.

### 2.1. Synthesis of pure PANI and NiO (NiO@PANI) composites

To synthesize the samples, we followed the strategy that was already reported in the literature (Scheme 1) [29]. Initially, solution A was prepared by adding 2.5 ml of aniline to 50 ml of distilled water. A few drops of HCl were added into solution A, which was then stirred for 30 minutes at a temperature below 20°C. In a separate beaker, solution B was prepared by dissolving 6.13 g of ammonium persulfate (APS) in 50 ml of distilled water and stirring it for 30 minutes. Subsequently, solution B was slowly added drop-wise into the solution. A while maintaining continuous stirring, resulting in solution C. Solution C was allowed to polymerize at room temperature for 24 hours. Following this, the precipitates were collected through centrifugation and washed successively with 1M HCl, deionized water, and ethanol until the filtrate became colorless. Finally, the collected product underwent vacuum drying at 60°C for 24 hours, yielding a dark green PANI powder. To synthesize NiO@PANI composites, the same procedure was followed as described above, with the addition of a stoichiometric amount of NiO nanoparticles before APS in solution C. For various NiO@PANI compositions, the amounts of NiO and PANI were adjusted as listed in Table S1. The samples obtained were labeled as follows: (a) Pure PANI, (b) Pure NiO, (c) NiO@PANI-2 containing 20% PANI, (d) NiO@PANI-4containing 40% PANI, (e) NiO@PANI-6 containing 60% PANI, and (f) NiO@PANI-8 containing 80% PANI. Scheme1 illustrates the procedure for preparing the NiO@PANI nanocomposites.

## 3. Materials characterizations

The X-ray diffraction (XRD) pattern of NiO@PANI has been analyzed with the help of a PANalytical X'pert PRO diffractometer containing Cu-K$\alpha$ rays '$\lambda$' is 1.54Å as a source of radiations operates at 30 mA to 40 K voltage sources. The SU8020 SEM/EDX was used to observe the synthesized samples surface morphology and detection of elemental analysis. The LCR meter (Model 895, Bench LCR Meters) was used for electrical measurements in the frequency range of 20 Hz to 1 MHz.

## 4. Results and discussion

### 4.1. Structural analysis

XRD characterization was performed to analyze the phase purity and crystal structure of as-synthesized NiO@PANI samples. In Fig. 2, the XRD patterns were successfully indexed with NiO, which exhibited a cubic structure with the Fm3m space group, matching well with standard JCPDS card no 22-1189. Furthermore, NiO nanoparticles maintain their crystalline structure even after being distributed throughout the PANI matrix. This could be attributed to the robust interaction between the PANI and NiO molecules. To investigate the lattice dynamics of the materials, the samples were refined using the Celref program version [30]. The magnitude of the peaks amplifies as the PANI content rises to 40% and declines after that. An upward trend in the lattice constants was found as the dopant content rose to a concentration of 40%, after which a fall was detected. Nevertheless, the trend exhibited a favorable divergence from Vegard's Law [31-32]. The Scherer formula was applied to determine the average crystallite size ($D$) in the samples [33]. The average particle size of synthesized samples can be calculated by using the Scherrer's formula an approximate value of 18.0 nm,

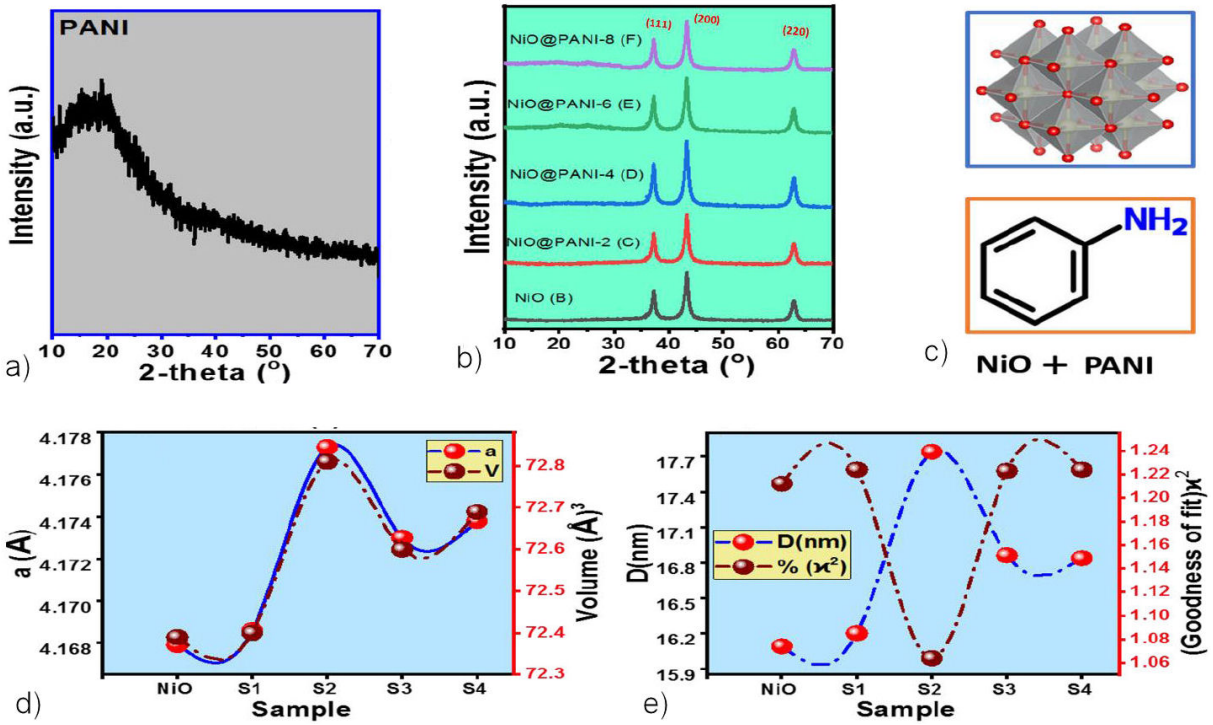


FIGURE 2. a) XRD Structure of Pure PANI b) XRD structure of NiO and NiO@PANI nanocomposites, c) NiO and PANI structure, d) Lattice parameters of NiO and NiO@PANI nanocomposites, e) Average crystallite size $D$ (nm) and Goodness of Fit ($\chi 2$).

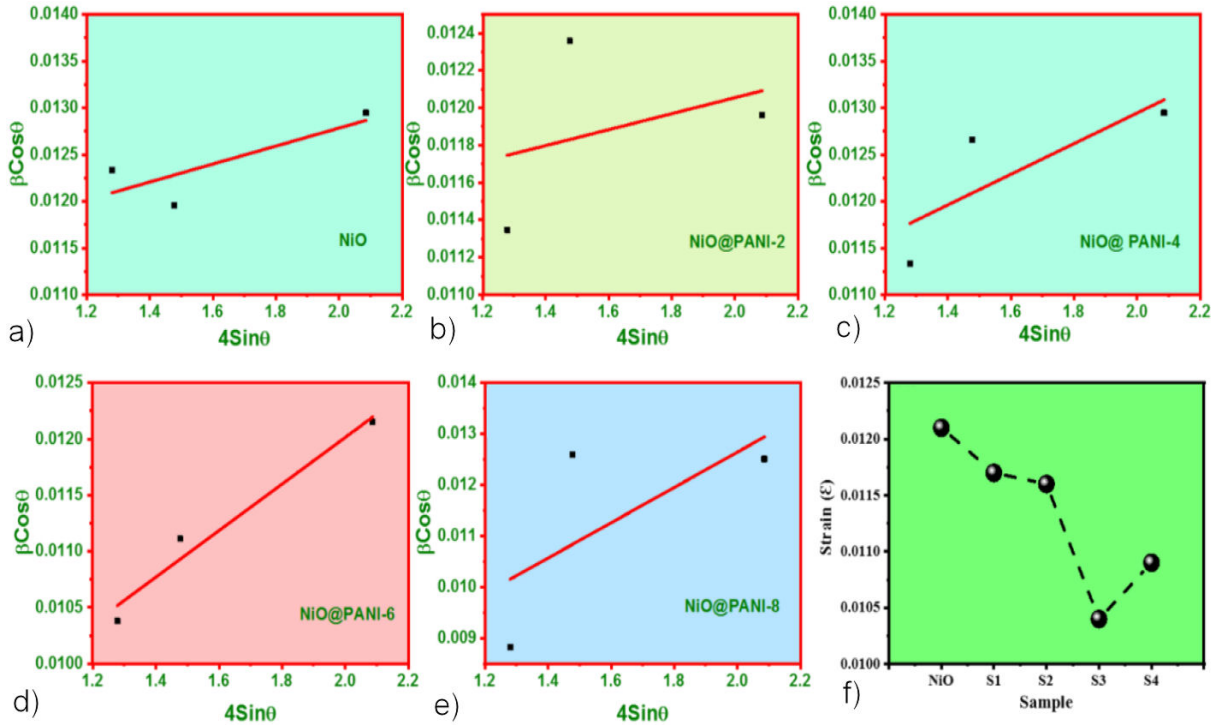


FIGURE 3. a)-e) Williamson-Hall Plots of NiO@PANI composites. f) Macrostrains of the synthesized nanocomposites.

18.2 nm, 18.7 nm, and 18.4 nm, and 18.5 for NiO, NiO@PANI-2, NiO@PANI-4, and NiO@PANI-6, NiO@PANI-8 respectively. Furthermore, the refinement process showed higher quality with lower values of the fitting parameter $\chi 2$. The correlation between the increase in intensity of the XRD patterns and the variation in size D could be established. In addition, W-H plots were employed to calculate macrostrains within crystallites, as illustrated in

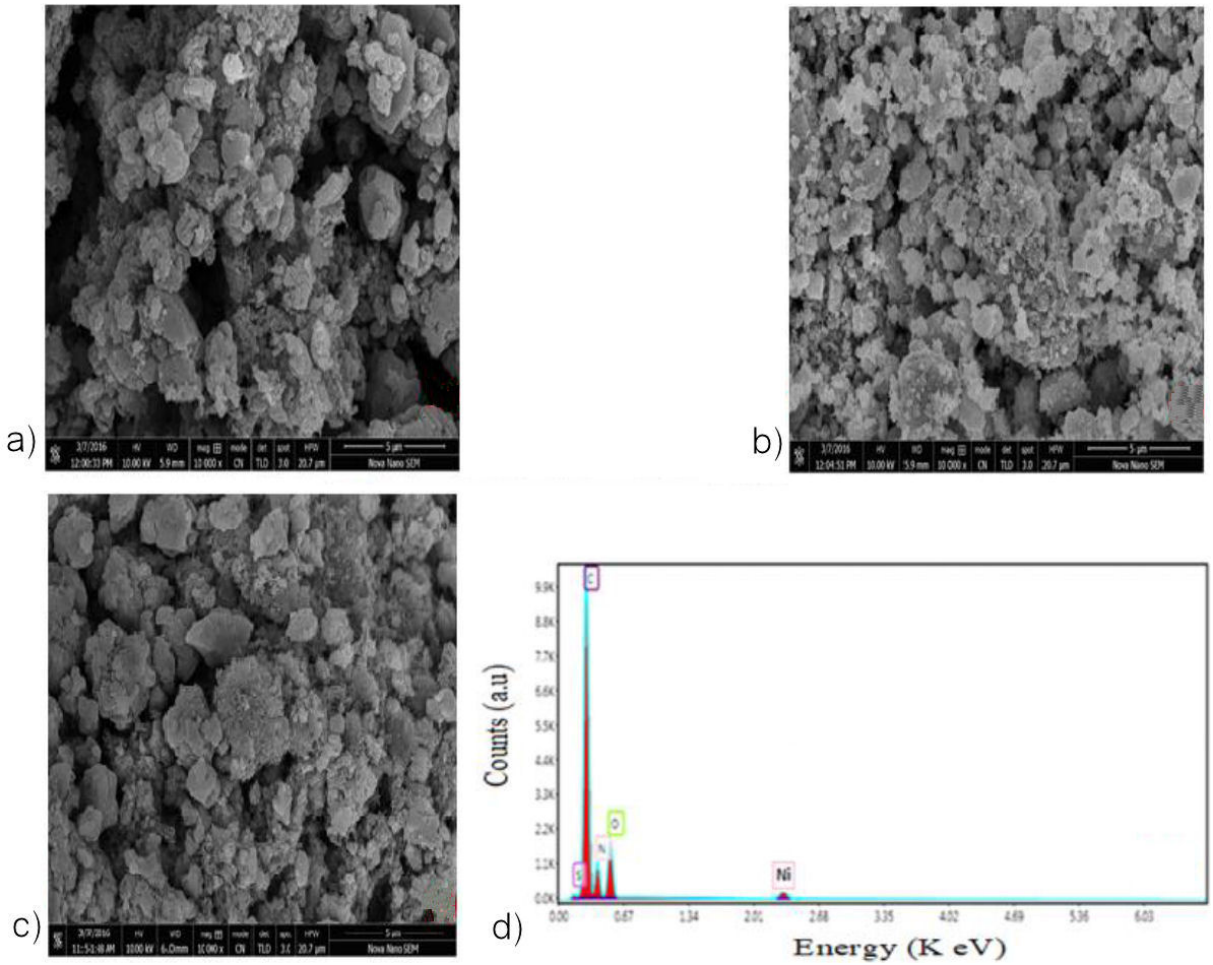


FIGURE 4. Morphological images of as-synthesized samples; a) pure PANI b) pristine NiO c) NiO@PANI nanocomposite d) EDX of NiO@PANI nanocomposite.

Figs. 3a)-3f). The Williamson-Hall (W-H) approach was utilized to compute the strain within crystallites and subsequently shown. The average size of the crystallites ($D = 19.0$ nm) of the NiO sample was also determined from the W-H plot. The overall strain exhibited a decline within the specified range as the dopants increased, indicating a compaction of the material [34-37].

### 4.2. SEM/EDX analysis

Figures 4a)-4d) exhibited the SEM images to analyze the surface morphology of pure PANI, pristine NiO and its nanocomposites. The micrograph of pristine PANI observed that the morphology of polyaniline volcanic rock type granular shaped and mesoporous. The SEM consequence shows that between the grains there is strong binding energy necessary to join the adjacent grains so there is a well-connected grain between the polyaniline molecules. In contrast, the pure NiO had a consistent spherical shape with a mesoporous microstructure [38]. The SEM image depicted small spherical particles. After analyzing the SEM images of all samples, including Pure PANI (a), Pure NiO (b) and (c)NiO@PANI have confirmed the formation of nanocomposite [39].

Analysis of the SEM images of NiO@PANI nanocomposites reveals that the addition of PANI to NiO particles results in a homogeneous distribution. Incorporating PANI macromolecules into NiO nanoparticles modifies the surface area of the nanocomposite [40-41]. The elemental composition of the selected sample was calculated using the EDX method. Figure 4d) shows EDX spectrum for NiO@PANI nanocomposite reporting the occurrence of C, N, O and S along with Ni elements. The measured quantitative data for all the elements is presented in Table I.

TABLE I. Elemental investigation of C, N, O, S and Ni.

| Elements | NiO@PANI nanocomposite |
|---|---|
| C | 58.40 |
| N | 11.68 |
| O | 9.55 |
| S | 8.67 |
| Ni | 11.70 |
| Total | 100 |

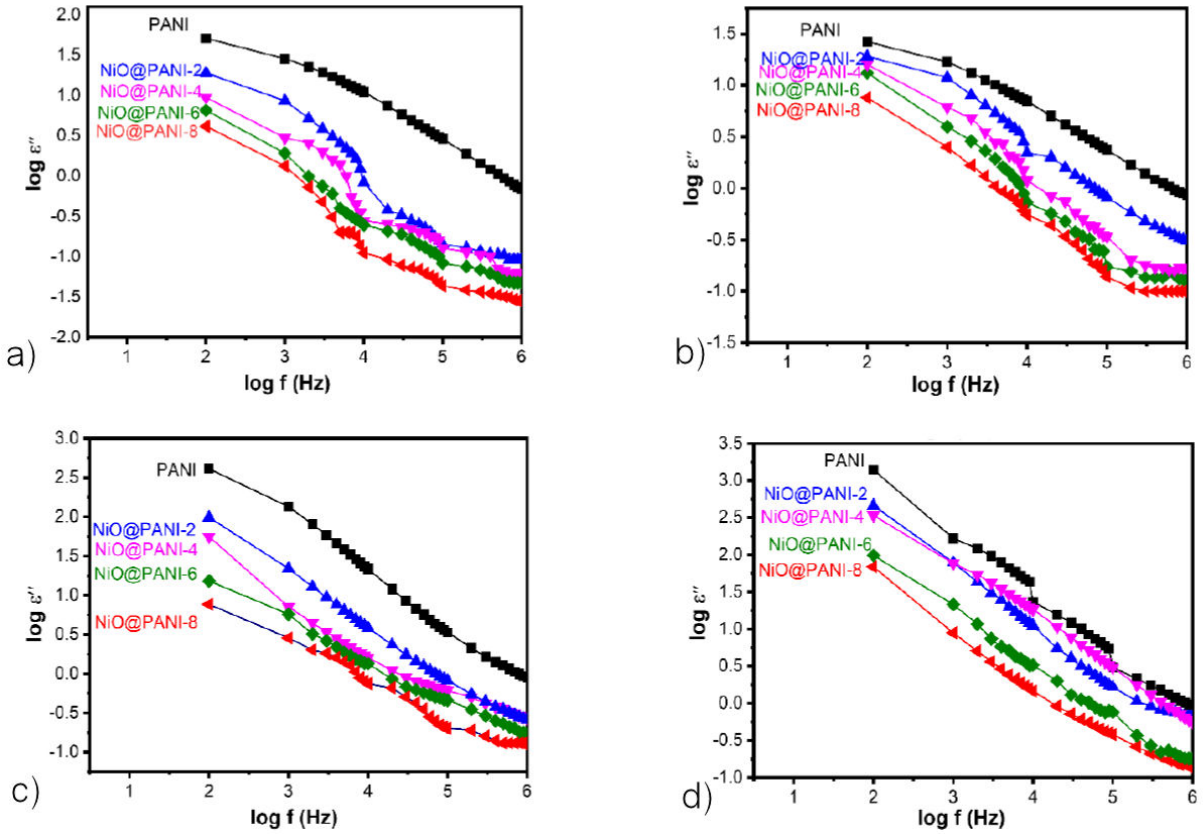


FIGURE 5. Frequency-dependent dielectric constant ($\log \acute{\varepsilon}$) of all the samples at a) room temperature, b) 40°C, c) 80°C, and d) 120°C.

### 4.3. Frequency dependent dielectric properties

#### *4.3.1. Dielectric constant*

Figure 5 depicts the correlation between the dielectric constant ($\varepsilon'$) and frequency, ranging from 20 Hz to 1 MHz, for PANI and NiO@PANI nanocomposites at both room temperature and higher temperatures. The dielectric constant ($\varepsilon'$) showed fluctuations in response to alterations in frequency, temperature, and NiO concentration [42-43]. The dielectric constant ($\varepsilon'$) demonstrates an inverse correlation with frequency, with higher values at lower frequencies and a significant decrease as frequency rises. As the frequency increases, the dielectric constant reaches a stable state and remains almost constant. The dielectric constant ($\varepsilon'$) is calculated using Eq. (1).

$$\varepsilon' = Cd/A\varepsilon_0. \tag{1}$$

The equation consists of the following variables: C denotes the capacitance, d is the thickness of the pellet, A denotes the area of the pellet, and $\varepsilon_0$ denotes the free space permittivity. Moreover, it was shown that the dielectric constant ($\varepsilon'$) rises as both the temperature and concentration of filler NiO increase, finally, at higher temperatures and frequency regions a linear trend was observed. With an increase in temperature, the intermolecular interactions that hold the polymer chains together become weaker, resulting in a higher level of thermal agitation. The increase in temperature results in a reduction in the duration of the relaxation process. Therefore, it modifies the polarization of dipoles. Moreover, the polymer chains tend to elongate with changing frequency, which may lead to an elevated dielectric constant [43].

#### *4.3.2. Dielectric loss*

Figure 6 depicts the correlation between frequency (ranging from 1 Hz to 1 MHz) and dielectric loss ($\varepsilon''$) for PANI and PANI-NiO nanocomposites at ambient temperature and higher temperatures. The dielectric loss ($\varepsilon''$) can be calculated by using Eq. (2).

$$\varepsilon'' = \varepsilon' \tan \delta. \tag{2}$$

Figure 7 shows that the values of $\varepsilon''$ exhibit an inverse relationship with frequency, the enhanced values of $\varepsilon''$ at lower frequencies and a decrease in $\varepsilon''$ values at higher frequencies and temperatures were observed [44]. The increase in $\varepsilon''$ at low frequencies is due to inducing the number of charge carriers at the interfaces that can produce a more significant number of dipoles at the interface. Increasing the number of dipoles can significantly influence the total polarization of the ionic medium, hence increasing the dielectric constant ($\varepsilon'$). At higher frequencies, the dipoles cannot promptly react to the applied AC field owing to inadequate relaxation time. As

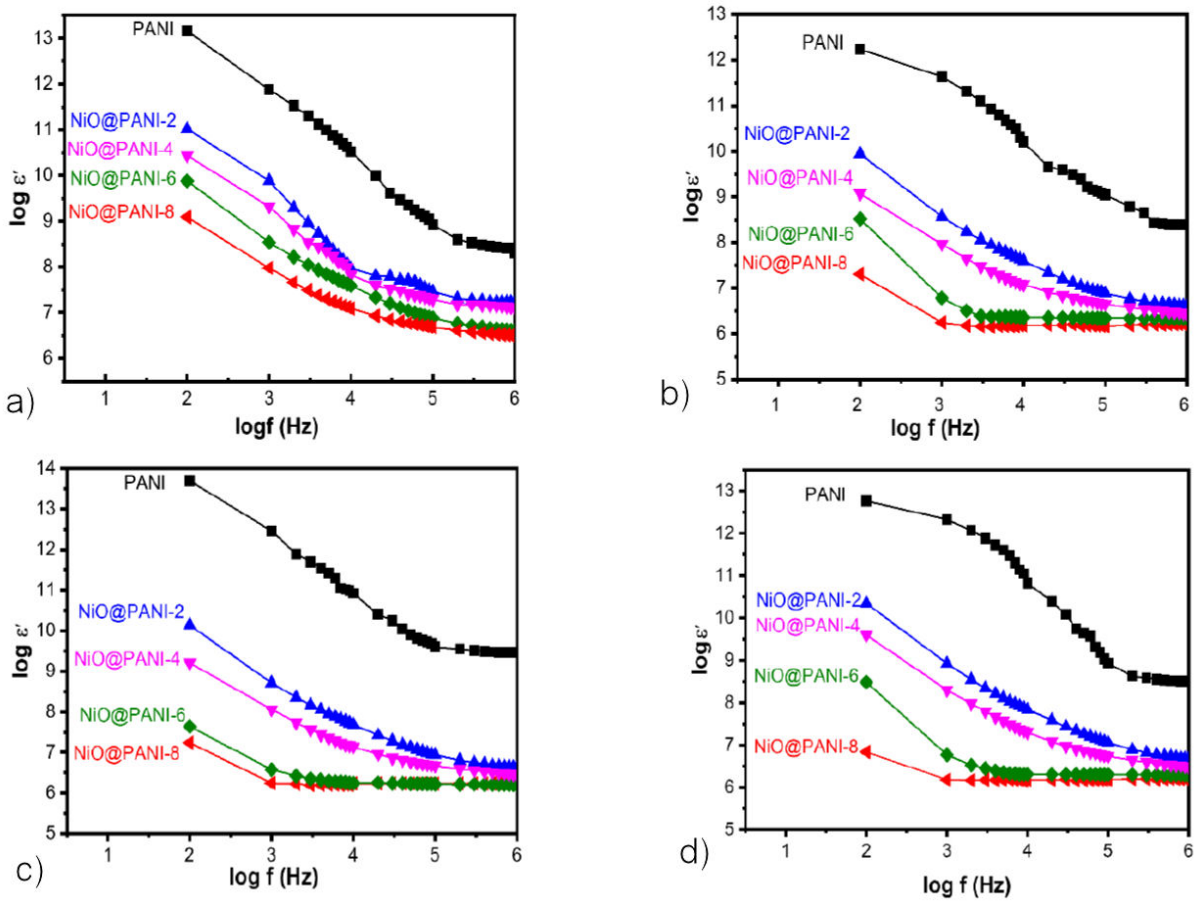


FIGURE 6. Frequency-dependent dielectric loss ($\log \dot{\varepsilon}$) of all the samples at a) room temperature, b) 40°C, (c) 80°C, and (d) 120°C.

a result, the surface polarization will decrease, causing a reduction in the values of $\varepsilon''$. Polarization, whether atomic or electronic, typically manifests at higher frequencies [45].

Figures 5a)-5b) show that the fundamental component of the dielectric constant ($\varepsilon'$) and the imaginary part of the dielectric constant ($\varepsilon''$) exhibit the lowest values at lower temperatures and lower concentrations of NiO in PANI. Both the real component ($\varepsilon'$) and the imaginary component $\varepsilon''$ demonstrate the substantial dispersion at lower frequencies due to the space charge polarization process. It was seen that the rise in ionic conductivity occurs due to the accumulation of charge carriers at the interface between the sample and electrodes. Where $\varepsilon'$ represents the energy stored, and $\varepsilon''$ represents the energy lost in each cycle of the applied field. At higher temperatures, the relative permittivity exhibits higher values at low frequencies, but at higher frequencies, it remains virtually constant [46]. The increase in dielectric constant and loss can be ascribed to the existence of localized mobile charges, which can induce interfacial dipoles via electric polarization. At higher frequencies, dipoles do not have enough time to relax ($Tr$) and align with the field, and their behavior is not affected by frequency. The static dielectric constant, denoted as ($\varepsilon' s$), represents the frequency-independent values [47]. At lower frequencies, dipoles have sufficient time to orient themselves in the same direction as an applied field, leading to a rise in the static dielectric constant behavior that depends on the frequency. In the equation ($f < f_r = 1/2\pi Tr$), the dipoles align themselves with an applied field in each dispersion zone. Here, $f_r$ represents the average relaxation frequency, and $\varepsilon'_r$ is equal to $\varepsilon'_s$. The dielectric properties are affected by the interaction with the AC field such as electronic, interfacial, dipolar, and atomic polarization, contributing to the basic mechanism [48]. This phenomenon can be ascribed to the charge transfer mechanism that takes place in the valence states of positively charged ions [49]. At higher frequencies, the dipoles do not respond to the applied AC field, resulting in a slight decrease in $\varepsilon'_r$. According to the relaxation frequency formula $fr = 1/2\pi Tr$ (where $Tr$ is the relaxation period), when the relaxation period occurs, the dipoles lose their ability to obey the applied field, leading to a notable decrease in both $\varepsilon'$ and $\varepsilon''$. The higher values of $\varepsilon'$ and $\varepsilon''$ observed at lower frequencies, as opposed to higher frequencies, can be ascribed to various forms of polarization process, encompassing electrode, interfacial, dipolar, atomic, ionic, and electronic.

The elevated values of $\varepsilon'$ and $\varepsilon''$ were observed at lower frequencies can be attributed to Maxwell Wagner polarization in heterogeneous systems [50-53].

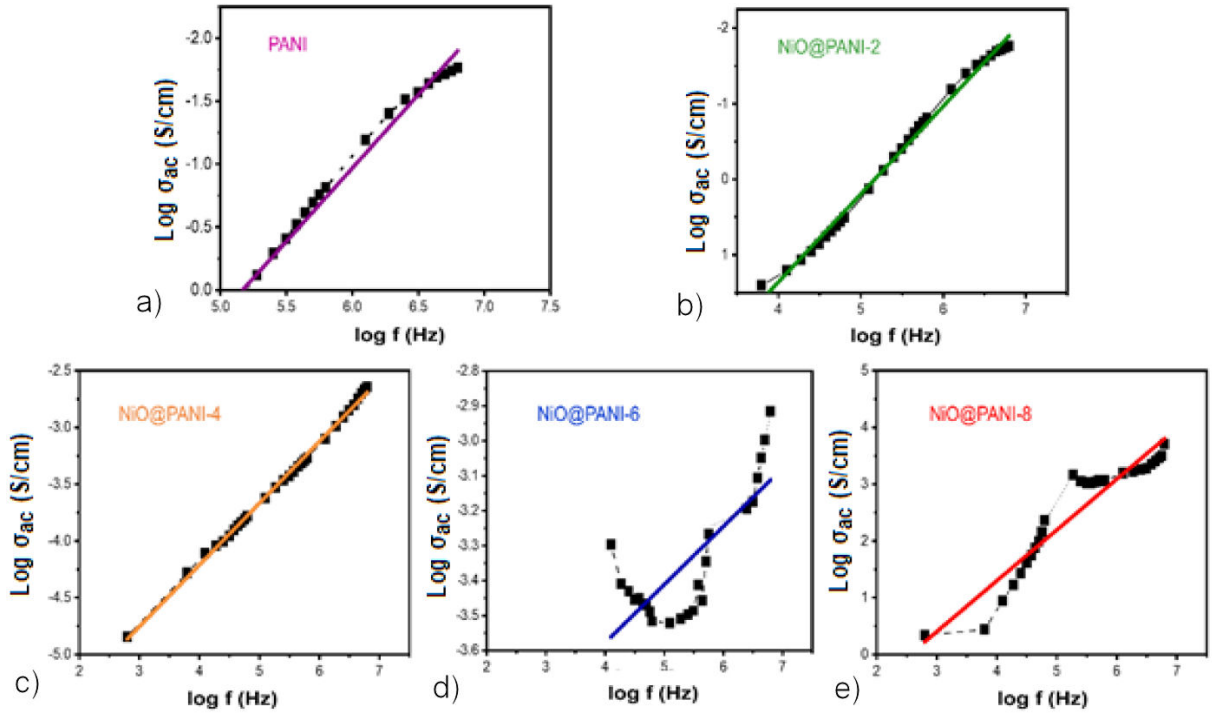


FIGURE 7. AC conductivities of the samples a) PANI b) NiO@PANI-2 c) NiO@PANI-4 d) NiO@PANI-6 e) NiO@PANI-8.

### 4.4. AC conductivity ($\sigma_{AC}$)

Figure 7 depicts the correlation between AC conductivity ($\sigma_{AC}$) and frequency, ranging from 20 Hz to 1 MHz, for all samples at room temperature and an elevated temperature. Equation (4) was utilized to calculate the alternating current conductivity ($\sigma_{AC}$) for both PANI and NiO@PANI nanocomposites.

$$\sigma_{AC} = 2\pi f \varepsilon o \varepsilon''. \tag{3}$$

The increase in AC conductivity was observed at high frequency, and elevated temperature ranges can be ascribed to the migration of polarons and bipolarons along the polymer chains.

According to the Maxwell-Wagner model, the conducting particles in all samples are detached by thin layers of grain boundaries that have a significant resistance. Grain boundaries cause a reduction in AC conductivity in low-frequency and temperature regions. However, Jonscher's power law Eq. (4) confirms the fundamental connection between frequency and AC conductivity (S/cm) [54-57].

$$\sigma_{\text{tot}}(\omega) = \sigma_{\text{DC}} + A\omega^n. \tag{4}$$

The symbol $\sigma_{\text{DC}}$ denotes the direct current conductivity, where $n$ represents the fractional exponent of a dimensionless factor, and A represents the pre-exponential factor measured in units of electrical conductivity. As $n$ approaches zero, the electrical conductivity converges to the DC conductivity and becomes frequency-independent. Therefore, the total conductivity can be obtained by summing the direct current (DC) conductivity and alternating current (AC) conductivity. It is clear from Fig. 7 that the AC conductivity is enhanced because the polarons and bipolarons are induced at elevated temperature and frequency [44].

## 5. Conclusion

The NiO@PANI nanocomposites were prepared using an in-situ polymerization method using varying weight percentages of PANI and NiO. The XRD analysis confirmed the structure of all samples. The SEM images revealed that the Nano hybrids exhibited a mesoporous morphology in the form of a spherical shape. The dielectric behavior of all the samples was studied. All the prepared samples follow Joncher's power law with a slope less than one, which confirms that the hopping conduction mechanism is prominent. The increase in dielectric constant, and reduction in the dielectric loss while an increase in AC conductivity for NiO@PANI nanocomposite was observed due to elongated polymer chains and induced maximum number of charge carriers. In comparison, NiO@PANI nanocomposite behaves as a semiconductor material and may be used as electrode material for charge storage devices and interrelated field applications.

## Acknowledgements

The authors would like to extend their sincere appreciation to the researcher supporting program project number (RSPD2025R1114) King Saud University, Riyadh, Saudi Arabia.

1. M. Kumar *et al*., Temperature dependent charge transport properties of polyaniline/NiO nanocomposite. *Materials Today: Proceedings*, (2023). https://doi.org/10.1016/j.matpr.2023.05.472.
2. K. Sarkar, A. Debnath, K. Deb, Effect of NiO incorporation in charge transport of polyaniline: improved polymer based thermoelectric generator. *Energy*, **177** (2019) 203, https://doi.org/10.1016/j.energy.2019.04.045.
3. L. Williams, A. Prasad, R. Sowmya, Characterization and temperature dependent DC conductivity study of bio templated nickel oxide nanoparticles (NiO) and their composites using polyaniline (PANI). *Materials Chemistry and Physics*,**242** (2020) 122469, https://doi.org/10.1016/j.matchemphys.2019.122469.
4. Y. Naik, V. Kariduraganavar, M. Y. Srinivasa, High surface wetting and conducting NiO/PANI nanocomposites as efficient electrode materials for supercapacitors. *Inorganic Chemistry Communications*, **138** (2022) 109275, https://doi.org/10.1016/j.inoche.2022.109275.
5. H. Taymaz, B. Eskizeybek, V. Kamıs, A novel polyaniline/NiO nanocomposite as a UV and visible-light photocatalyst for complete degradation of the model dyes and the real textile wastewater. *Environmental Science and Pollution Research*, **28** (2021) 6700, https://doi.org/10.1007/s11356-020-10956-0.
6. A. M. Azharudeen, R. Karthiga, M. Rajarajan and A. Suganthi, Fabrication, characterization of polyaniline intercalated NiO nanocomposites and application in the development of non-enzymatic glucose biosensor. *Arabian Journal of Chemistry*, **13** (2020) 4053, https://doi.org/10.1016/j.arabjc.2019.06.005.
7. S. Kailasa *et al*., NiO nanoparticles-decorated conductive polyaniline nanosheets for amperometric glucose biosensor. *Materials Chemistry and Physics*, **242** (2020) 122524. https://doi.org/10.1016/j.matchemphys.2019.122524.
8. K. P. Gautam *et al.*, Nickel Oxide-Incorporated Polyaniline Nanocomposites as an Efficient Electrode Material for Supercapacitor Application. *Inorganics*, **10** (2022) 86. https://doi.org/10.3390/inorganics10060086.
9. A. A. Ensafi, K. Z. Mousaabadi, R. Fazel-Zarandi, Application of Conductive Polymers in Electrochemistry. *ACS Symposium Series*, **1405** (2022) 185. https://doi.org/10.1021/bk-2022-1405.ch008.
10. H. S. Roy *et al*., Polyaniline-NiO nanocomposites as tunable conducting materials. *Materials Today: Proceedings*, **15** (2019) 380, https://doi.org/10.1016/j.matpr.2019.04.097.
11. S. Jamil *et al.*, Synthesis and characterization of polyaniline/nickel oxide composites for fuel additive and dyes reduction. *Chemical Physics Letters*, **776** (2021) 138713. https://doi.org/10.1016/j.cplett.2021.138713.
12. Furhan, K. Vyshakh, M. T. Ramesan, Enhanced optical properties, thermal transitions, temperature-dependent electrical properties and modelling studies of poly (diphenylamine)/NiO nanocomposites. *Journal of Materials Science*, **57** (2022) 18385. https://doi.org/10.1007/s10853-022-07759-8.
13. N. L. Singh, A. Qureshi, F. Singh, D. K. Avasthi, Effect of swift heavy ion irradiation on dielectrics properties of polymer composite films. *Materials Science and Engineering: B*, **137** (2007) 85, https://doi.org/10.1016/j.mseb.2006.10.013.
14. S. L. Goyal, S. Sharma, D. Jain, D. Kumar, N. Kishore, In situ synthesis and characterization of polyaniline/nickel oxide composites. *Advances in Applied Science Research*, **6** (2015) 89-98.
15. S. A. Ansari *et al.*, Temperature dependence anomalous dielectric relaxation in Co doped ZnO nanoparticles. *Materials Research Bulletin*, **47** (2012) 4161. https://doi.org/10.1016/j.materresbull.2012.08.079.
16. N. V. Iyer *et al*., Wet Chemical Feasible Synthesis of PPy-Nickel Oxide nanocomposites and their photocatalytic effects on Methylene Blue. *Journal of Water and Environmental Nanotechnology*, **8** (2023)23-33. https://doi.org/10.22090/jwent.2023.08.003.
17. Mahadeva, H. K. Inamdar, C. Sridhar B, Synthesis of NiO doped Polyaniline nanocomposites: Structural and DC conductivity studies. *Materials Today: Proceedings*, **68** (2022) 424, https://doi.org/10.1016/j.matpr.2022.06.575.
18. S. Seifikar *et al.*, Structural and magnetic properties of biaxially textured NiFe2O4 thin films grown on c-plane sapphire. *Journal of Applied Physics*, **112** (2012) 123910. https://doi.org/10.1063/1.4770366.
19. M. Jamdegni, A. Kaur, Highly efficient dark to transparent electrochromic electrode with charge storing ability based on polyaniline and functionalized nickel oxide composite linked through a binding agent. *Electrochimica Acta,* **331** (2020) 135359. https://doi.org/10.1016/j.electacta.2019.135359.
20. C. Huang et al., Synthesis of polyaniline/nickel oxide/sulfonated graphene ternary composite for all-solidstate asymmetric supercapacitor. *Applied Surface Science*, **505** (2020) 144589. https://doi.org/10.1016/j.apsusc.2019.144589.
21. M. Mohandesi, M. Tavakolian, M. R. Rahimpour, Eggplant as an appreciable bio-template for green synthesis of NiO nanoparticles: Study of physical and photocatalytic properties. *Ceramics International*, **48** (2022) 22820. https://doi.org/10.1016/j.ceramint.2022.04.157.
22. T. Munawar, M. S. Nadeem, F. Mukhtar, S. Manzoor, M. N. Ashiq, and F. Iqbal, Surfactant-assisted facile synthesis of petal-nanoparticle interconnected nanoflower like NiO nanostructure for supercapacitor electrodes material. *Materials Science and Engineering: B*, **284** (2022) 115900. https://doi.org/10.1016/j.mseb.2022.115900.
23. J. H. Lee *et al*., Room-temperature detection of acetone gas by PANI/NiOloaded TiO2 nanoparticles under UV irradiation. *Sensors and Actuators B: Chemical, 374* (2023) 132850, https://doi.org/10.1016/j.snb.2022.132850.

24. C. Pawar *et al*., Development of Mixed Metal Oxides-Conductive Polymer Composites for an Anticorrosive Application. *Arabian Journal for Science and Engineering*, **48** (2023) 7841. https://doi.org/10.1007/s13369-023-07911-9.

25. M. A. Sayed *et al*., Photocatalytic hydrogen generation from raw water using zeolite/polyaniline Ni2O3 nanocomposite as a novel photo-electrode. *Energy*, **187** (2019) 115943. https://doi.org/10.1016/j.energy.2019.115943.

26. A. L. Jadhav, S. L. Jadhav, A. V. Kadam, Effect of Different Metals Doped in Nickel Oxide Nanomaterials on Electrochemical Capacitive Performance. *Supercapacitors for the Next Generation*, **1** (2021) 879. https://doi.org/10.5772/intechopen.99326.

27. V. Babel, B. L. Hiran, A review on polyaniline composites: Synthesis, characterization, and applications. *Polymer Composites*, **42** (2021) 3142. https://doi.org/10.1002/pc.26048.

28. P. Elumalai, J. Charles, Investigation of structural and optical properties of ternary polyaniline-polypyrrole-nickel oxide (PANI-PPy-NiO) nanocomposite for optoelectronic devices. *Polymer International*, **72** (2023) 176, https://doi.org/10.1002/pi.6456.

29. S. U. Asif *et al.*, Phonon vibrations and photoluminescence emissions and their correlations with the electrical properties in Er3+ doped Bi3YO6 oxide-ion conductors. *Solid State Ionics*, **344** (2020) 115092, https://doi.org/10.1016/j.ssi.2019.115092.

30. S. U. Asif *et al.*, Impact of Ferromagnetic Ni Substitution on Structural and Magnetic Parameters of $Ba_{0.8}In_{0.2}Fe_{12-x}Ni_xO_{19}$ ($x$ = 0.00-2.00) Hexaferrites. *Journal of Inorganic and Organometallic Polymers*, **33** (2023) 2721. https://doi.org/10.1007/s10904-023-02713-w.

31. S. Asif, U. Ranjha, Q. A. Ghori, U. R. Nisa, Exploring the structural and magnetic trends in $Ba_{0.9}Sm_{0.1}Fe_{12-x}Al_xO_{19}$ M-type Hexaferrites. *Physica Scripta*, **98** (2023) 015836, https://doi.org/10.1088/1402-4896/acac54.

32. B. Alshammari *et al*., Structural and magnetic conduct in Sm and Al substituted $Ba_{0.9}Sm_{0.1}Fe_{10}Al_2O_{19}$ M-type hexaferrites at different sintering temperatures. *Physica Scripta*, **98** (2023) 065905. https://doi.org/10.1088/1402-4896/acce7a.

33. B. I. Nandapure, S. B. Kondawar, M. Y. Salunkhe, A. I. Nandapure, Magnetic and transport properties of conducting polyaniline/nickel oxide nanocomposites. *Advanced Materials Letters*, **4** (2013) 134, https://doi.org/10.5185/amlett.2012.5348.

34. M. E. Mazhar *et al*., Insight into the Structural Characterization of Pure and Zr-doped Hydrothermally Synthesized Cerium Oxide Nanoparticles. *Materials Research Express*, *6* (2019) 105022, https://doi.org/10.1088/2053-1591/ab0f5f.

35. M. M. Lumina Sonia, S. Anand, V. M. Vinosel, M. Asisi Janifer, S. Pauline, Effect of lattice strain on structural, magnetic and dielectric properties of sol-gel synthesized nanocrystalline Ce 3+ substituted nickel ferrite. *Journal of Materials Science: Materials in Electronics*, **29** (2018) 15006, https://doi.org/10.1007/s10854-018-9639-2.

36. H. Irfan, K. Mohamed Racik, S. Anand, Microstructural evaluation of CoAl2O4 nanoparticles by Williamson-Hall and size-strain plot methods. *Journal of Asian Ceramic Societies*, **6** (2018) 54. https://doi.org/10.1080/21870764.2018.1439606.

37. S. Anand, S. Pauline, Vinosel, and V. M. Janifer, Structural rietveld refinement and vibrational study of M-type $BaFe_{12}O_{19}$ nanoparticles. *Materials Today: Proceedings*, **8** (2019) 476, https://doi.org/10.1016/j.matpr.2019.02.141.

38. Y. D. Xia and R. Mokaya, Ordered mesoporous carbon hollow spheres nanocast using mesoporous silica via chemical vapor deposition. *Advanced materials*, **16** (2004) 886, https://doi.org/10.1002/adma.200306448.

39. F. Fazlali, A. reza Mahjoub, R. Abazari, A new route for synthesis of spherical NiO nanoparticles via emulsion nanoreactors with enhanced photocatalytic activity. *Solid State Sciences*, **48** (2015) 263, https://doi.org/10.1016/j.solidstatesciences.2015.08.022.

40. A. C. Sonavane *et al*., Multicoloured electrochromic thin films of NiO/PANI. *Journal of Physics D: Applied Physics*, **43** (2010) 315102. https://doi.org/10.1088/0022-3727/43/31/315102.

41. R. S. Diggikar, S. P. Deshmukh, T. S. Thopate, S. R. Kshirsagar, Performance of polyaniline nanofibers (PANI NFs) as PANI NFssilver (Ag) nanocomposites (NCs) for energy storage and antibacterial applications. *ACS Omega*, **4** (2019) 5741. https://doi.org/10.1021/acsomega.8b02834.

42. K. S. Ngai, S. Ramesh, K. Ramesh, J. C. Juan, A review of polymer electrolytes: fundamental, approaches and applications. *Ionics*, **22** (2016) 1259. https://doi.org/10.1007/s11581-016-1756-4.

43. B. Sun, Y. Li, Ubiquitous clean and sustainable energy-driven self-rechargeable batteries realized by and used in organic electronics. *Journal of Materials Chemistry C*, **10** (2022) 388. https://doi.org/10.1039/D1TC04122C.

44. Z. Wang, X. Wang, S. Cong, F. Geng, Z. Zhao, Fusing electrochromic technology with other advanced technologies: A new roadmap for future development. *Materials Science and Engineering: R: Reports*, **140** (2020) 100524. https://doi.org/10.1016/j.mser.2019.100524.

45. Z. Lu, X. Zhong, X. Liu, J. Wang, X. Diao, Energy storage electrochromic devices in the era of intelligent automation. *Physical Chemistry Chemical Physics*, **23** (2021) 14126. https://doi.org/10.1039/d1cp01398j.

46. T. Prasse, J. Y. Cavaille, W. Bauhofer, Electric anisotropy of carbon nanofibre/epoxy resin composites due to electric field induced alignment. *Composites Science and Technology*, **63** (2023) 1835. https://doi.org/10.1016/S0266-3538(03)00019-8.

47. H. R. Vutukuri *et al*., An experimental and simulation study on the selfassembly of colloidal cubes in external electric fields. *Soft Matter*, **10** (2014) 9110. https://doi.org/10.1039/c4sm01778a.

48. S. Zaineb, S. Atiq, A. Mahmood, S. M. Ramay, S. Riaz, S. Naseem, Thermal tuning of electrical and dielectric characteristics of Mn-doped $Zn_{0.95}Fe_{0.05}O$ dilute magnetic semiconductors. *Journal of Materials Science: Materials in Electronics*, **29** (2018) 3943. https://doi.org/10.1007/s10854-017-8334-z.

49. H. S. Roy, Md. M. Islam, M. Y. A. Mollah, Md. A. B. Hasan Susan, Polyaniline-NiO nanocomposites as dielectric materials. *Materials Today: Proceedings*, **5** (2018) 15267. https://doi.org/10.1016/j.matpr.2018.05.005.

50. B. Rajashekhar *et al.*, Synthesis, Characterization and Study of Electrical Properties of Polyaniline-NiO Nanocomposites, *IJREAS*, **1** (2015). http://13.232.72.61:8080/jspui/handle/123456789/717.

51. Y. Liu, H. Xing, L. Wang, Z. Liu, H. Wang, H. Jia, Novel microwave absorption materials of porous flower-like nickel oxide polyaniline in the X-band. *Nano* **13** (2018) 1850059, https://doi.org/10.1142/S1793292018500595.

52. J. Lu, K. S. Moon, B. K. Kim, and C. P. Wong, High dielectric constant polyaniline/epoxy composites via in situ polymerization for embedded capacitor applications. *Polymer* **48** (2007) 1510, https://doi.org/10.1016/j.polymer.2007.01.057.

53. X. Wu, Q. Wang, W. Zhang, Y. Wang, W. Chen, Nano nickel oxide coated graphene/polyaniline composite film with high electrochemical performance for flexible supercapacitor. *Electrochimica Acta*, **211** (2016) 1066. https://doi.org/10.1016/j.electacta.2016.06.026.

54. W. Abbas *et al*., Electrochemical determination of urinary dopamine from neuroblastoma patients based on Cu nanoplates encapsulated by alginatederived carbon. *Journal of Electroanalytical Chemistry*, **853** (2019) 113560. https://doi.org/10.1016/j.jelechem.2019.113560.

55. W. Abbas *et al*., Study of the Electrical Properties and Electrochemical Sensing Efficiency of Hydrothermally Synthesized Sr Doped Nickel Oxide Nanomaterials. *Physica Scripta*, **97** (2022) 075004. https://doi.org/10.1088/1402-4896/ac74ed.

56. W. Abbas *et al*., Facilely green synthesis of 3D nano-pyramids Cu/Carbon hybrid sensor electrode materials for simultaneous monitoring of phenolic compounds. *Sensors and Actuators B: Chemical*, **282** (2019) 617. https://doi.org/10.1016/j.snb.2018.11.114.

57. R. Megha *et al*., Effect of mechanical mixing method of preparation of polyaniline-transition metal oxide composites on DC conductivity and humidity sensing response. *Journal of Materials Science: Materials in Electronics*, **29** (2018) 7253. https://doi.org/10.1007/s10854-018-8714-z.